

Alma Mater Studiorum Università di Bologna
Archivio istituzionale della ricerca

Towards sustainability in 3D printing of thermoplastic composites: Evaluation of recycled carbon fibers as reinforcing agent for FDM filament production and 3D printing

This is the final peer-reviewed author's accepted manuscript (postprint) of the following publication:

Published Version:

Giani N., Mazzocchetti L., Benelli T., Picchioni F., Giorgini L. (2022). Towards sustainability in 3D printing of thermoplastic composites: Evaluation of recycled carbon fibers as reinforcing agent for FDM filament production and 3D printing. COMPOSITES. PART A: APPLIED SCIENCE AND MANUFACTURING, 159, 1-12 [10.1016/j.compositesa.2022.107002].

Availability:

This version is available at: <https://hdl.handle.net/11585/887688> since: 2024-01-17

Published:

DOI: <http://doi.org/10.1016/j.compositesa.2022.107002>

Terms of use:

Some rights reserved. The terms and conditions for the reuse of this version of the manuscript are specified in the publishing policy. For all terms of use and more information see the publisher's website.

This item was downloaded from IRIS Università di Bologna (<https://cris.unibo.it/>).
When citing, please refer to the published version.

(Article begins on next page)

This is the final peer-reviewed accepted manuscript of:

N. Giani, L. Mazzocchetti, T. Benelli*, F. Picchioni, L. Giorgini ***“Towards sustainability in 3D printing of thermoplastic composites: evaluation of recycled carbon fibers as reinforcing agent for FDM filament production and 3D printing”*** *Composites: Part A* **159**, 107002 (2022) <https://doi.org/10.1016/j.compositesa.2022.107002>

The final published version is available online at:
<https://www.sciencedirect.com/science/article/pii/S1359835X22001907?via%3Di%3Dhub>


Terms of use:

Some rights reserved. The terms and conditions for the reuse of this version of the manuscript are specified in the publishing policy. For all terms of use and more information see the publisher's website.

This item was downloaded from IRIS Università di Bologna (<https://cris.unibo.it/>)

When citing, please refer to the published version.

Towards sustainability in 3D printing of thermoplastic composites: Evaluation of recycled carbon fibers as reinforcing agent for FDM filament production and 3D printing

 The corrections made in this section will be reviewed and approved by a journal production editor.

Niccolò [Giani](#)^a, Laura [Mazzocchi](#)^{a,b,c,*}, laura.mazzocchi@unibo.it, Tiziana [Benelli](#)^{a,b,c,*}, tiziana.benelli@unibo.it, Francesco [Picchioni](#)^d, Loris [Giorgini](#)^{a,b,c}

^aDepartment of Industrial Chemistry “Toso Montanari”, University of Bologna, Viale Risorgimento 4, 40136 Bologna, Italy

^bInterdepartmental Center for Industrial Research on Advanced Applications in Mechanical Engineering and Materials Technology, CIRI-MAM, University of Bologna, Viale Risorgimento 2, 40136 Bologna, Italy

^cINSTM UDR Bologna, Via Giusti 9, Firenze, Italy

^dFaculty of Science and Engineering (FSE), University of Groningen, Nijenborgh 9, 9747 AG Groningen, Netherlands

Q3 *Corresponding author at: Department of Industrial Chemistry “Toso Montanari”, University of Bologna, Viale Risorgimento 4, 40136 Bologna, Italy.

*Corresponding author at: Department of Industrial Chemistry “Toso Montanari”, University of Bologna, Viale Risorgimento 4, 40136 Bologna, Italy.

Abstract

The use of recycled Carbon Fibers (*r*CFs) into polylactic acid (PLA) matrix to produce new reinforced 3D printing filaments was assessed. Filaments containing 5 and 10 wt% of *r*CFs were manufactured and, in order to compare the effect of the partial oxidized surface of recycled CFs on the adhesion with PLA matrix, filaments of pure PLA and with the same concentration of washed virgin Carbon Fibers (*v*CFs) were also produced. As expected the addition of CFs impacts the 3D printed thermal and mechanical properties, leading to the reduction of thermal expansion up to 85% and to a substantial increase of the storage modulus up to 7.1 GPa for PLA/*v*CF10. Furthermore this study underlines that the use of *r*CFs leads to a thermo-mechanical performance well comparable with that of the analogue virgin fibers based materials, supporting the suitability of recycled CFs for 3D printing applications. Indeed, when the fiber aspect ratio is not a crucial detrimental point, the quality of recycled CFs has now achieved performances that make them a better alternative to the pristine fibers, in particular when economic aspects are also taken into account.

Keywords:

Recycled carbon fibers, Polylactic acid, Additive manufacturing, Thermoplastic composites

Abbreviations

No keyword abbreviations are available

1 Introduction

Since the 1970 s Carbon Fiber Reinforced Composites (CFRCs) are replacing more and more conventional materials in high performance applications thanks to their lightweight and excellent mechanical properties [1,2]. Accordingly, the demand for CFRCs, that grew from 128,500 tons in 2018 to 141,500 tons in 2019, is foreseen to be about 197,000 tons in 2023 [3]. However, next to the huge boost in their production and applications, one of the main unsolved issues is still their disposal, both at the end-of-life and as production of scraps waste irrespective of the matrix type, being it a thermoset or a thermoplastic [4,5]. Furthermore, the production of Carbon Fibers (CFs) is extremely highly energy requiring (183–286 MJ/kg) [6] thus they are a high-priced material, with minimum price of 30–40€/kg.[7] Hence, the ability to recover CFRCs, and recycle the CFs, i.e. the highest added value fraction of the composite, to re-use them, seems to be a promising option in terms of sustainability and circular economy. In this regard pyro-gasification of CFRCs appears as a very favourable process to recycle carbon fibers from composites [8,9]. The two-steps process starts with pyrolysis of waste composites (either cured or uncured), leading to an almost complete degradation of the polymeric matrix and a solid residue of recycled CFs (*r*CFs) covered by a thin layer of residual char. An additional mild oxidation step, gasification, has to be applied in order to remove the residual char layer and leave a clean *r*CFs surface. Moreover, it has been found that this oxidation step brings out an oxygen-rich surface on the fiber that might result in an improved adhesion toward slightly hydrophilic polymer matrices in the new applications of *r*CFs [9,10,11]. It is worth nothing that the overall process can be almost energetically self-sustained, when considering the energy recovery from valorisation of the volatile pyrolytic fractions [12,13,14]. This recycling technology allows to obtain CFs with significant reduced cost (up to about 10€/kg [15]) which could be used in the place of virgin CFs (*v*CFs) leading to advantages both from the economic and environmental point of view. Considering that a neat PLA filament for 3D printing costs around 15€/kg, a CF-reinforced filament is priced about twice as much (over 30€/kg). In this context, the substitution of *v*CF with *r*CF would bring a significant reduction of the cost of composite filaments. The overall recycling process, however, will find reliable industrial application only if the produced *r*CFs can find new applications, bypassing the scepticism associated to re-use of such a high performing material. The main issue still related to the recycling of CFRCs is the heterogeneity of feeding materials, since scraps and end-of-life products have irregular shapes, resulting in *r*CFs with different length. This challenge imposes a reuse of *r*CFs in the form of short fibers to provide a uniform reinforcing agent of homogeneous shape. In this regard, application of *r*CFs in Additive Manufacturing (AM), mainly Fused Deposition Modelling (FDM), a process that requires a CFs length less than 1 cm to prevent printing troubles [16], appears a promising field.

The use of CFs composites for AM processed in FDM is not a new topic, and many thermoplastic polymers, such as, among the others, amorphous and semicrystalline polymers as acrylonitrile–butadienestyrene polymer (ABS) [17,18,19,20] or polylactic acid (PLA) [17,21,22], as well as nylon or polypropylene already applied to the production of continuous fiber filaments [23,24], have been already reported and used in this field. PLA is one of the most state-of-the art material in FDM [25,26] because of its good mechanical properties, printability, biocompatibility [27] and biodegradability [28,29,30,31] which allow its application also in biomedical and food packaging fields. Among the benefits of mixing CFs in PLA matrix in FDM, there are the increase of mechanical properties, such as elastic modulus and tensile strength [17], more efficient cooling of extruded material [32,33], which leads to a better accuracy of details, and decrease of Coefficient of Thermal Expansion (CTE) [19,33]. Nevertheless, the use of CFs in FDM, as consequence of the boosted cooling of the material during printing, provokes the reduction of interlayer strength that leads to an enhanced anisotropy of 3D printed parts [17,21,34]. It is also renown that adding carbon fibers to a polymer leads to a decrease in CTE, as well as an increase in thermal conductivity, which could substantially reduce the *warping* and dimensional inaccuracies of printed parts [19,32,33].

In this context the use of *r*CFs produced by recycling of consolidated CFRP waste composites in a semi-industrial plant [10,11] has been studied as reinforcing agent to produce a composite 3D printing filament. Indeed, while some works were reported on the use of recycled thermoplastics for AM processes [35,36], the aim of the paper is to prove that recycled carbon fibers can replace pristine ones in FDM, in a context where the initial shortened dimension of the fiber does not play a detrimental role. So, filaments composed of neat PLA, as reference material, and filaments containing 5 and 10 wt% of *r*CFs, without any additional treatment after recycling process, have been manufactured. Moreover, in order to evaluate the effect of the partially oxidized surface of recycled CFs on the adhesion with PLA matrix, filaments with the same concentration of washed virgin CFs (*v*CFs), i.e. lacking the slight surface oxidation [11], have also been produced for the sake of comparison. All filaments have been studied in terms of thermal properties, via Differential Scanning Calorimetry (DSC) and Thermogravimetric Analysis (TGA), fiber/polymer composition and fibers length distribution. 3D printed specimens have been then produced and characterized via Dynamic Mechanical Analysis (DMA) and tensile tests along two printing directions (0° and 90°). Finally, the Coefficient of Linear Thermal Expansion (CTE) was also measured on 3D printed specimens (0° and 90°).

2 Experimental section


2.1 Materials

Poly(lactic acid) (PLA), Ingeo™ 4043D from NatureWorks, USA (Melt flow rate of 6 g/10 min, 210 °C, 2.16 Kg) was used as matrix. Recycled CFs (*r*CFs) were kindly supplied by Curti SpA (Castelbolognese, Italy) and derive from pyro-gasification of consolidated CFRP waste epoxy composites based on T700 carbon fibers in a semi-industrial pilot plant [11]. Such plant does not require any preliminary shredding or pre-treatment of the waste composites. Consolidated CFRP were provided by Bucci Composites srl (Faenza IT) and treated in a semi industrial pyro-gasification pilot plant able to treat up to 70 Kg CFRP per batch. The treatment has been carried out at 500 °C both for the pyrolysis and the gasification treatments. *r*CFs were cut down (7 mm) by a chopper gun. Virgin chopped carbon fibers (*v*CFs) (7 mm), were obtained cutting down Unidirectional Fabric UC 301 based on Toray T700S 12 K dry fabrics kindly provided by Bucci Composites (Faenza, Italy). *v*CFs, before use, were washed twice with acetone at reflux for 2 days, in order to remove the sizing agent. Acetone and chloroform were purchased by Sigma Aldrich and used without further purification.

2.2 Filament processing and 3D printing

Starting materials (neat PLA pellets, and CFs) were first dried in a vacuum oven at 105 °C for 5 h. They were compounded in different matrix/fibers ratios (Table 1) by two-step thermal processes. A double-screw mixer PLASTICORDER® (Brabender™, Germany) was used for melt mixing the materials at 170, 175 and 180 °C (respectively for neat PLA, PLA/CF5 and PLA/CF10) with a screw speed up to 100 rpm. Chopped CFs, either washed virgin or recycled, were added to neat PLA after 2 min and further compounded for 5 minutes [37]. Subsequently, the composites were ground in a cutting mill (Brabender™, Germany) with square sieve perforations of 4 × 4 mm² and reprocessed in a Next 4.0 Advanced (3Devo, The Netherlands) *single-screw* extruder with 4 heating zones (165–170–175–165 °C) using a screw speed up to 8 rpm. This extruder is equipped with an optical sensor that allows to obtain 3D-printable filaments with the desired diameter (1.75 mm).

Table 1

 The table layout displayed in this section is not how it will appear in the final version. The representation below is solely purposed for providing corrections to the table. To preview the actual presentation of the table, please view the Proof.

Produced filaments.

Sample	Reinforcement	Reinf. Conc. (% wt)
Neat PLA	–	–
PLA/ <i>r</i> CF5	<i>r</i> CF	5
PLA/ <i>v</i> CF5	<i>v</i> CF	5
PLA/ <i>r</i> CF10	<i>r</i> CF	10
PLA/ <i>v</i> CF10	<i>v</i> CF	10

Specimens for further characterization were 3D printed with a Mustang M400 printer (Vepam Vetoplast s.a.s., Italy) at 230 °C, with a heated bed at 60 °C, 20 mm/s printing speed, 0.2 mm layer height, 100% infill and using a nozzle diameter of 0.6 mm. Both specimens for tensile test and CTE measurements were printed using 2 different deposition angles, one parallel and the other perpendicular to the direction of mechanical stress application, namely 0° and 90°.

2.3 Characterization methods

Thermal stability and CFs content of composite filaments were investigated by Thermogravimetric Analysis (TGA) carried out on a TA Instrument SDT Q600 at 20 °C/min from room temperature to 500 °C under nitrogen flow (100 mL/min) and leaving them in isotherm for 15 min. TGA runs intended for CFs content determination were carried out in triplicate for each sample, on approximately 20 mg of filaments taken at least 50 cm apart one from the other. T_o is the onset degradation temperature and W_r the residual weight.

Differential Scanning Calorimetry (DSC) measurements were performed on a TA Instruments Q2000 DSC Modulated apparatus equipped with RCS cooling system and calibrated with Indium standards. Heating scans were run at 10 °C/min from 0 °C to 220 °C, in a nitrogen atmosphere. Between heating scans, a constant rate cooling (10 °C/min) was applied. Crystallization temperature (T_c) and melting temperature (T_m) were taken at the peak maximum of endotherm and exotherm, respectively. In the presence of multiple endotherms, the temperature of the most intense peak was taken as T_m . The degree of crystallinity (χ) was evaluated as the ratio of initial crystallinity of the material - defined as the ΔH_m at the beginning of the heating scan, calculated as total melting enthalpy subtracted of the cold crystallization enthalpy, $(\Delta H_m - \Delta H_c)$ - and the theoretical melting enthalpy of 100% crystalline PLA ($\Delta H_{m,0} = 93.7$ J/g [38]) according to Eq. (1).

$$\chi(\%) = \frac{(\Delta H_m - \Delta H_c)}{\Delta H_{m,0}} * 100 \quad (1)$$

DSC runs were carried out in triplicate for each sample, on approximately 5 mg of filaments. Q2000 DSC Modulated apparatus was used also for determination of the specific heat capacity (C_p). The analysis was carried out by setting the heat flow at 30 °C equal to zero (target temperature for C_p measurement), using a sampling interval of 1pt/sec and heating the sample from 10 °C to 50 °C (heating rate of 10 °C/min). A calibration using a sapphire standard sample was required to assess the heat capacity of the instrument cell prior each set of analyses. The analysis has been carried out in triplicate for each formulated filament.

Determination of average CFs length was performed upon dissolution of small amount of composite filament (about 5 g) in CHCl_3 at room temperature. The solubilized polymer was filtered off and the collected CFs were washed 4 times with chloroform, dried in oven at 75 °C for 24 hours and observed using an optical microscope (Imager A1, Zeiss).

The Dynamic Mechanical Analysis (DMA) of printed specimens was carried out using a DMA model 242E Artemis (Netzsch, Germany). Three bar-shaped ($40 \times 4 \times 1.4$ mm) specimens for each formulation were tested in tensile mode heating from 30 °C to 100 °C (heating rate 3 °C/min) with 1 Hz oscillation frequency, 5.0 N dynamic force, 0.1 N constant static force, 1.1 proportional factor (PF, ratio of static force to dynamic force) and 50 μm strain. $E_{30^\circ\text{C}}^I$ is the elastic modulus at 30 °C, T_{onset} the onset temperature of modulus drop and $\tan\delta$ the loss factor.

The Coefficient of Linear Thermal Expansion (CLTE) [39] was measured using the above-mentioned DMA apparatus pre-set in TMA mode, in tensile deformation. After preliminary calibration with a standard steel specimen carried out in the exact same conditions of the CTE evaluation, printed specimens were tested applying a static force of 0.05 N during the analysis and heating from 30 to 100 °C (heating rate 3 °C/min). The same shape of DMA specimen ($40 \times 4 \times 1.4$ mm) was used. The probe displacement (dL) was recorded and CLTE was calculated as reported in Eq. (2):

$$CLTE(\alpha) = \frac{\Delta L}{\Delta T} * \frac{1}{L_0} \quad (2)$$

where L_0 is the initial gauge length of specimens (about 10 mm, carefully defined for each specific specimen).

Tensile tests on 3D-printed dumbbell specimens were carried at RT with an Instron-type tensile testing machine (REMET TC10) equipped with a 10 kN load cell, using a crosshead speed of 1 mm/min. Three specimens were tested for each formulation. Surface fracture images were taken with a scanning electron microscope (SEM) ZEISS EVO 50 EP in environmental mode with ≈ 100 Pa pressure in the chamber, after graphitization of the surface. In the case of filaments, they were kept in liquid nitrogen for 10 min prior submitting them to fragile fracture. 3D printed broken specimens at mechanical testes were analysed without any further treatment.

3 Results and discussion


Carbon fibers, when dispersed in a thermoplastic matrix, do not form strong, covalent bonds as it might happen with conveniently sized fibers in suitable thermosets. Nonetheless, CFs can positively interact with a thermoplastic matrix and provide improved thermomechanical properties, depending strongly on the fibers size and extent of alignment. Van de Werken et al. [32] predicted the impact of CFs length, namely the aspect ratio of CFs, on mechanical properties of an additively manufactured composite using theoretical models. The study revealed a minimum critical CF length of 7 mm to provide at least 80% of the theoretical maximum mechanical properties of bulk CF-composite. Consequently, in the present work CFs were initially chopped down to about 7 mm length. However, it has already been observed in the literature [40] that, owing to the composite fabrication process involving machining steps that might lead to CFs breakage, the average fiber length in 3D-printed parts ends up being around 100 μm . Since recycled CFs could be more brittle than virgin ones [10] the final fiber dimension after the whole production procedure had to be reassessed, in order to evaluate if the recycled fibers were suffering harsher consequences than virgin ones. Composite filaments were compounded in a *double-screw* mixer, ground with an electric grinder and reprocessed in a *single-screw* extruder with the aim to obtain uniform compositions. Different attempts were made at optimizing processing conditions that finally led to PLA/rCF5 and PLA/rCF10 3D-printable filaments, i.e. filaments containing 5 and 10% wt of recycled carbon fibers respectively, collected as spool with a controlled 1.75 mm diameter. Such a double extrusion process is adopted to ensure homogeneity in the filament composition [40]. A similar processing was used also to produce neat PLA filaments, in order to subject the polymer to the exact same thermal treatment. For the sake of comparison, the same formulations containing washed vCFs with no sizing on the surface, instead of recycled ones, were also produced, with

the aim to evaluate the effect of surface oxidation on the properties of the final composite materials. Indeed, as reported by Li et al. [41], an active CF surface could enhance compatibility between CF and PLA matrix, leading to a decrease in micro-voids and mechanical properties improvement. So, since the pyro-gasification of CFRCs was found to be able to produce recycled CFs with a partially oxidized surface [10], the use of *r*CFs in the production of 3D printing PLA filaments would have not only a positive impact in terms of sustainability, but it could also lead to improved mechanical properties owing to an intrinsic enhanced adhesion with the matrix without requiring additional sizing treatments [11].

3.1 Filament characterization

All the composites' formulations (Table 1) were obtained as filaments and, at a first glance, the addition of the reinforcement led to an improvement in the consistency of the filament diameter and ovality, possibly owing to the higher thermal conductivity of CFs that may homogenise the cooling process during filament production. This resulted also in a more homogeneous filament diameter distribution, as evaluated in more than 30 points along the whole filament produced. Only a segment of PLA-*v*CF5 filament showed some diameter fluctuations, but in order to guarantee the same processing condition the filament was used anyway. With the aim to, at least, roughly estimate the CFs content, as well as the overall thermal stability of the composites, all the obtained filaments were analysed by TGA adopting a temperature program able to selectively degrade the polymeric matrix without significant CFs damage [42]. Results of the tests are summarized in Table 2.

Table2

 The table layout displayed in this section is not how it will appear in the final version. The representation below is solely purposed for providing corrections to the table. To preview the actual presentation of the table, please view the Proof.

Thermal stability, CFs content, average length and specific heat capacity of formulated filaments.

Sample	T _o (°C) ^a	W _r (% wt) ^b	CF length (μm)	C _p , 30 °C (J/°C * g)
Neat PLA	328 ± 3	–	–	1.40 ± 0.07
PLA/ <i>r</i> CF5	326 ± 2	5 ± 1	200 ± 100	1.34 ± 0.08
PLA/ <i>v</i> CF5	324 ± 4	6 ± 1	190 ± 120	1.36 ± 0.01
PLA/ <i>r</i> CF10	332 ± 2	11 ± 1	170 ± 100	1.20 ± 0.05
PLA/ <i>v</i> CF10	332 ± 1	10 ± 1	150 ± 60	1.26 ± 0.04

Table Footnotes

^a Onset degradation temperature determined by TGA.

^b CFs content measured by TGA.

All composite filaments show a similar thermodegradative behaviour, with a single weight loss beginning above 320 °C for all the samples (*Figure SII* in [Supplementary Information](#)). The filaments, however, differ mainly in their residue at 500 °C, that primarily depends on their composition (*SII-Figure SII* and [Table 2](#)). In particular, as reported in [Table 2](#), the CFs content well compares with the feed, suggesting a good homogeneity of the obtained filaments. As previously reported by Tekinalp et al. [20], the thermal stability of PLA shows a slight enhancement when 10 wt% of CFs is added (PLA/*r*CF10 and PLA/*v*CF10). Such a behaviour could be attributed to the high thermal conductivity of CFs, which facilitates heat dissipation within the composite [43].

With the aim of evaluating the effect of the compounding procedure on the CFs length, the dispersed fibers had to be separated from the matrix. While the TGA residue is mainly composed of CFs and could in principle be used for such a purpose, the CFs integrity upon handling after thermal treatment cannot be guaranteed. Hence samples of the composite filaments were dissolved in CHCl₃ and the recovered solid residue, composed of unaltered CFs, was analysed by optical microscopy ([Fig. 1](#)). The fibers breakage was expected, and indeed observed ([Table 2](#)), with all the formulations showing a severe drop in the average fibers length (from 7 mm to 150–200 μm), whose entity seems to lightly increase with the CFs content. Although longer fibers would lead to a much larger improvement of mechanical properties [32], they could provoke printing troubles, such as an irregular extrusion or even the clogging of the nozzle. The achieved length is, instead, slightly higher than the average literature reported results (100 μm) [32,40] and suitable for the 3D printing, since the nozzle diameter is 600 μm. Moreover, it is worth to note that the use of recycled CFs with respect to virgin CFs did not cause a more severe CF breakage. With the aim of evaluating the CFs dispersion and alignment, the section of composite filaments was analysed by SEM after fragile fracture. As shown in [Fig. 2](#), all filaments containing the 5 and 10 wt% of CFs display a rather homogeneous reinforcement dispersion, as evidenced by the average even spacing of fibers as inferred by their extremities emerging from the surface and their counterparts, i.e. fiber pull out cavities: neither CF agglomerations nor voids were detected. Moreover, as already reported by Jiang et al. [44], SEM

images highlight also a strong CFs prevailing alignment in the direction of the extrusion flow creating an almost unidirectional reinforcement inside the filament [44], with no significant differences between *v*CFs and *r*CFs. These findings suggest that the optimized mixing process allows to produce homogeneous composite filaments reinforced with well dispersed recycled or virgin CFs with comparable average length.


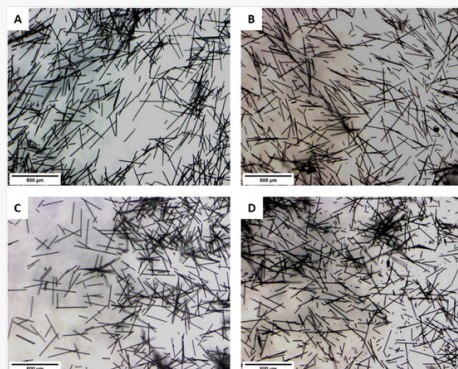
 Images are optimised for fast web viewing. Click on the image to view the original version.

Fig. 1



Optical microscope images of CFs deriving from dissolution of produced composite filaments in CHCl_3 : PLA/*r*CF5(A), PLA/*v*CF5 (B), PLA/*r*CF10 (C) and PLA/*v*CF10 (D). The scale bar indicates 500 μm .


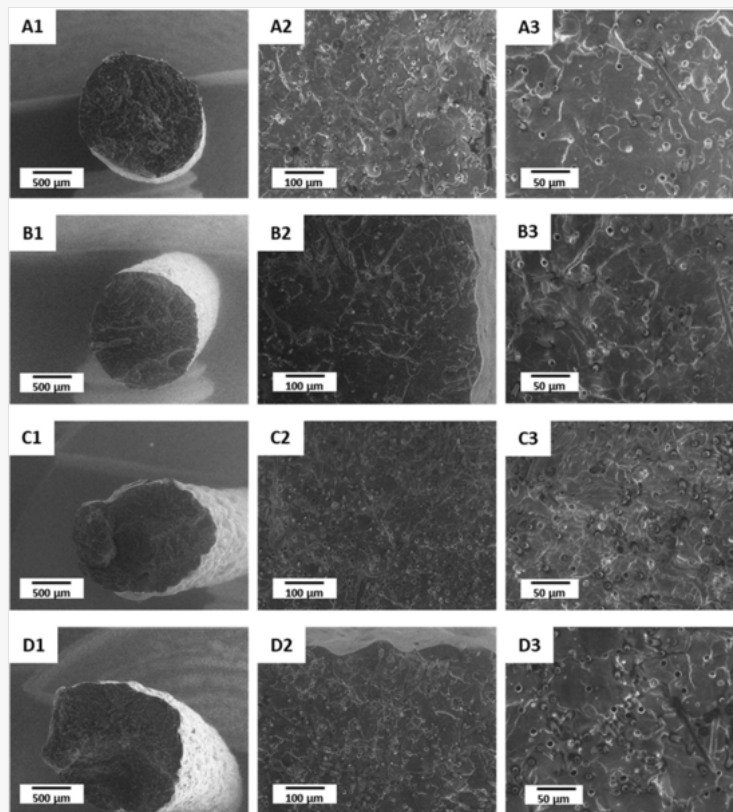
 Images are optimised for fast web viewing. Click on the image to view the original version.

Fig. 2



SEM images of cryogenic fractured surface of composite filaments: PLA/rCF5 (A), PLA/vCF5 (B), PLA/rCF10 (C) and PLA/vCF10 (D). Numeration indicates the used magnification: 100× (1), 500× (2) and 1000× (3).

All the composite filaments were investigated also by DSC. For the sake of comparison, the starting PLA pellet and neat PLA filament were analysed too, and all the relevant curves are reported in Fig. 3, while data are summarized in Table 3. DSC thermogram of the PLA pellet first heating scan (Fig. 3-A) shows a stepwise transition, ascribed to PLA glass transition temperature (T_g) located at 59 °C, followed by an intense endothermic peak at 153 °C, typical of PLA melting. In the second heating scan (Fig. 3-B), only the stepwise transition remains. Neat PLA filament, instead, shows in the first scan, in addition to the T_g , whose evaluation is hampered by the presence of an overlapping strong enthalpic relaxation, a broad exothermic transition of low intensity at about 130 °C, which can be ascribed to a *cold crystallization* [21,38], typical of semi-crystalline polymers characterized by a low crystallization rate, prior an endothermic peak of about the same intensity. The same behaviour is observed in the second heating scan, with less intense transitions. A very similar trend is observed, both in the first and second heating scans, for all the composite filaments (Fig. 3-A and -B): the cold crystallization enthalpy (ΔH_{cc}) increases from 15 J/g for PLA filament to over 25–35 J/g for CFs reinforced PLA filaments in the 1st scan and from 6 J/g to over 20–30 J/g in the 2nd ones (Table 3). Such a behaviour can be attributed to the nucleating effect of CFs [38], that also contributes to the lowering of the crystallization (T_{cc}) and melting temperature (T_m) and once again it seems that no significant difference is observed between vCFs and rCFs. Contrarily, there is a slight effect of the amount of added fibers, with a somehow stronger impact on T_{cc} and T_m at higher fiber content, however irrespective of the fiber origin, i.e. vCFs or rCFs. The T_g , instead, is practically unaffected by the CFs addition to PLA in all the filaments, as shown in Table 3. It is worth to point out that DSC measurements confirm that all the obtained filaments are essentially amorphous, with crystallinity

values around 1%. DSC was also used to evaluate the specific heat capacity (C_p) at 30 °C for all the filaments, and the measured values are reported in Table 2. C_p is evaluated for all the samples along the direction of extrusion, that is the direction of CFs prevailing alignment. Indeed, the efficiency of heat dissipation is a crucial property in 3D printing materials because the presence of a temperature gradient in the 3D printed part during printing process could lead to an inhomogeneous cooling of the material and, in turn, to *warping*. Polymeric materials are usually good insulators, characterized by low thermal conductivity and high specific heat capacity, and so they are not able to disperse efficiently the heat leading to the formation of hot spots in the 3D printed object during the process. Fig. 4 displays the specific heat capacity trend for all the filaments around the target temperature, that in this case is set at 30 °C: this is the temperature at which the heat flow is set to be zero in the calibration run, thus providing the absolute value for the C_p of the analysed specimens. Thermograms clearly show that the addition of CFs to the neat PLA leads to a decrease of C_p (from 1.40 of neat PLA to 1.20 of PLA/rCF10 filament), whose entity depends on the amount of fibrous filler. Such a behaviour can be ascribed to the extremely low specific heat capacity of carbon-based reinforcement, that from Toray T700 technical datasheet is about 0.75 J/g °C [45]. This value is not expected to change significantly with recycling process, if anything could just slightly improve [46,47], since the graphitic content is not observed to change dramatically [10]. As reported in the literature [32,48] such a low C_p ends up decreasing the specific heat capacity of the composites as a function of CFs content. These results are very promising for 3D printing process because it might lead to higher thermal conductivity along the fiber direction, which tends to minimize temperature gradients during the cooling of the printed part, and thus the warping.


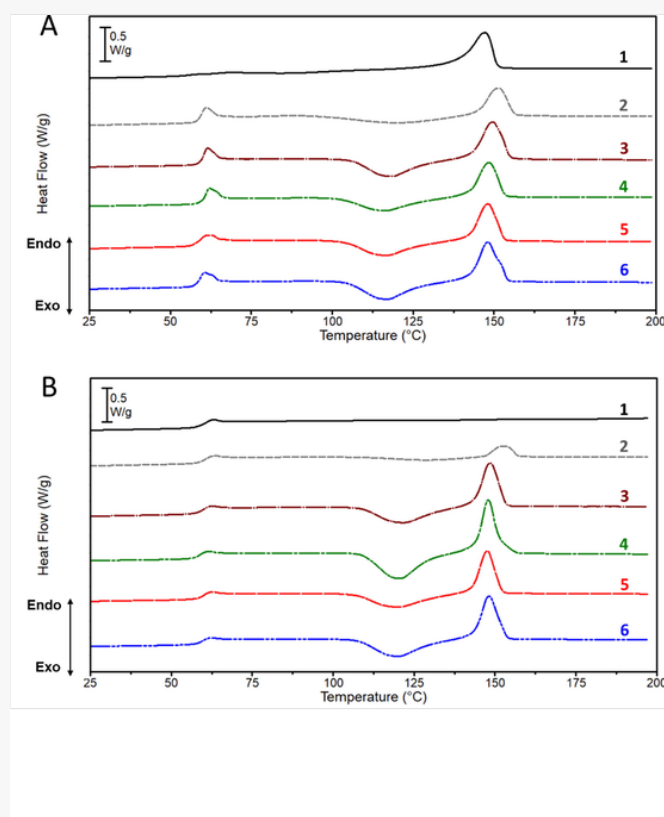

 Images are optimised for fast web viewing. Click on the image to view the original version.

Fig. 3



DSC thermograms (1st and 2nd heating scans, A and B respectively) of (1) PLA pellet (—), (2) Neat PLA (---), (3) PLA/rCF5 (— · —), (4) PLA/vCF5 PLA (— · — · —), (5) PLA/rCF10 (— · — · — · —) and (6) PLA/vCF10 (— · — · — · — · —) filaments. Thermograms displayed are representative of each batch of specimens. (For interpretation of the references to colour in this figure legend, the reader is referred to the web version of this article.)

Table 3

 The table layout displayed in this section is not how it will appear in the final version. The representation below is solely purposed for providing corrections to the table. To preview the actual presentation of the table, please view the Proof.

DSC results relative to 2nd heating scan of PLA pellets and formulated filaments.

Sample	T_g (°C)	T_{cc} (°C)	ΔH_{cc} (J/g)*	T_m (°C)	ΔH_m (J/g)*	χ_c (%)

PLA pellet	59	–	–	–	–	0
Neat PLA	59	129	6.1 ± 0.5	153	6.9 ± 0.4	0.9 ± 0.7
PLA/ <i>r</i> CF5	59	122	24.1 ± 0.2	149	25.4 ± 0.2	1.5 ± 0.4
PLA/ <i>v</i> CF5	59	124	24.1 ± 0.6	150	25.6 ± 0.2	1.6 ± 0.4
PLA/ <i>r</i> CF10	59	120	21.5 ± 0.3	147	23.1 ± 0.5	1.7 ± 0.3
PLA/ <i>v</i> CF10	58	120	24.9 ± 0.3	148	25.9 ± 0.5	1.0 ± 0.3

*Crystallization and melting enthalpy (ΔH_c and ΔH_m) are normalized with the real polymer content in the composite material.


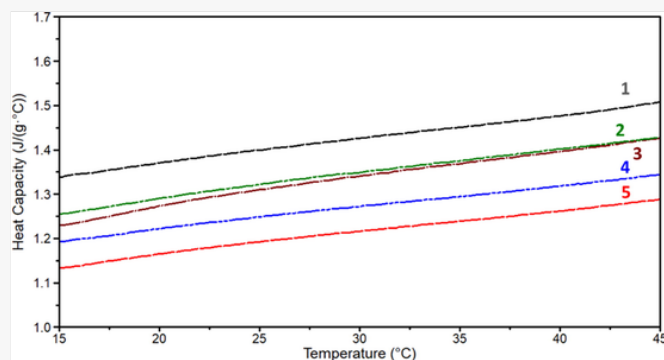
 Images are optimised for fast web viewing. Click on the image to view the original version.

Fig. 4



Specific heat capacity thermograms of filaments: (1) Neat PLA (---), (2) PLA/*v*CF5 PLA (—○—), (3) PLA/*r*CF5 (—○—), (4) PLA/*v*CF10 (—○—) and (5) PLA/*r*CF10 (—○—). Curves displayed in the figure are representative of each batch of specimens. (For interpretation of the references to colour in this figure legend, the reader is referred to the web version of this article.)

3.2 3D printed specimens production and characterization

The produced filaments were used to manufacture 3D printed specimens for further characterization. Different specimens were manufactured, in order to evaluate the printability of the filaments and to investigate mechanical properties of 3D printed structures. In particular, bars (40x4x1.4 mm) were prepared for both DMA and CLTE evaluation, instead dog-bone specimens (ASTM D638 *Type V*) were 3D printed to perform mechanical testing. Furthermore CLTE bars and dog-bones were 3D printed adopting two different printing deposition angles, one parallel and the other perpendicular to either the direction of mechanical stress application or of the evaluation of linear expansion in CTE, namely 0° and 90°, in order to highlight tensile properties (0°) and layer adhesion quality (90°) of the composites. Printed samples are displayed in SI2-Figure SI2. Specimens were printed as reported in the Experimental section. Initially a 0.4 mm nozzle diameter was used to obtain a good quality of the printed part, but the presence of CFs led to frequent nozzle clogging, especially for 10 wt% CFs filaments. So, to attain a stable printing process, a 0.6 mm nozzle diameter was adopted. Specimens produced with neat PLA filaments, in the applied conditions started to warp already during the third layer printing, probably owing to a too fast cooling of printed material. The problem was solved increasing the temperature of the heated bed to 60 °C. CF-reinforced PLA filaments, except PLA-*v*CF5 filament, show good printability using same parameters of neat PLA and no further adjustment was required. Since PLA-*v*CF5 filament displayed a light diameter fluctuation, toward thinner sections, in this regard the 3D printing required further adjustment of printing parameters, such as the light reduction of the printing speed and a slight increase of the extrusion flow.

The 1st heating scan of the DSC analysis (SI2-Figure SI3) was used to investigate actual thermal properties of all the produced materials after 3D printing. The observed behaviour is summarized in Table 4 and is strongly reminiscent of the features already discussed about the filaments and previously reported in Table 3 and Fig. 3. Indeed, 3D printed samples were totally amorphous, with a crystallinity degree (χ_c) that ranges from 0% to 2%, thanks to the fast cooling involved in the printing process. Even the cold crystallization/melting behaviour is analogous to the filaments, though 3D printed specimens show crystallization enthalpies slightly higher than the corresponding filaments. Unlike filaments, the T_g of 3D printed parts was affected by the presence of CFs (Table 4) showing a drop of 4–5 °C compared to the reference material (PLA 4043D). Such a behaviour suggests that the 3D printed multi-layered structure is influenced by the presence of CFs.

Table 4

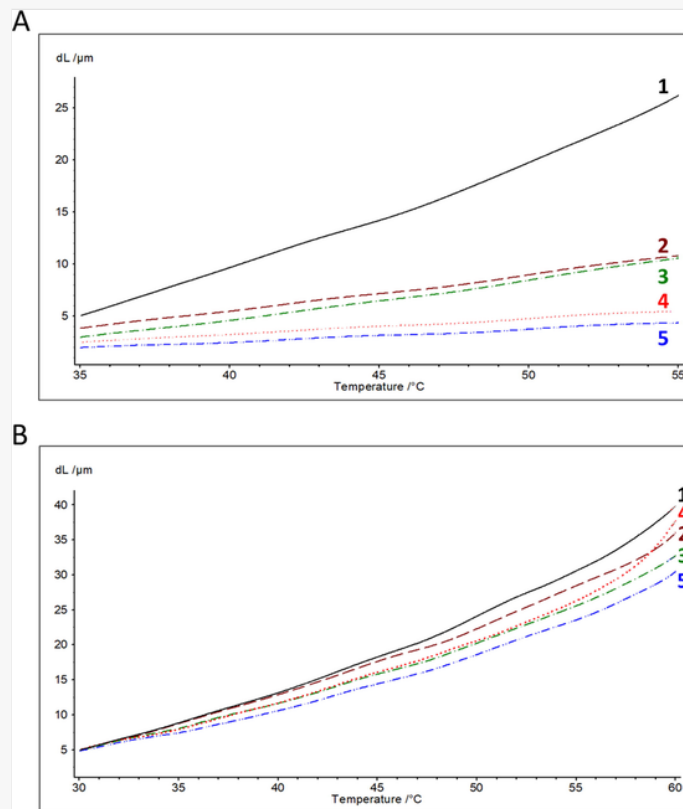
DSC and CLTE results for all 3D printed samples.

Sample	DSC				CLTE			
	T _g (°C)	T _{cc} (°C)	ΔH _{cc} * (J/g)	T _m (°C)	ΔH _m * (J/g)	χ _c (%)	Deposition angle	CLTE (10 ⁻⁶ 1/K)
Neat PLA	59	120	15.9 ± 2.1	150	17.0 ± 1.2	1	0°	104.6 ± 4.7
							90°	109.9 ± 1.2
PLA/ <i>r</i> CF5	55	117	28.7 ± 0.3	149	28.4 ± 0.5	0	0°	35.1 ± 1.1
							90°	97.5 ± 5.6
PLA/ <i>v</i> CF5	55	117	27.6 ± 0.1	149	29.0 ± 0.7	1	0°	38.2 ± 1.6
							90°	87.6 ± 1.5
PLA/ <i>r</i> CF10	55	119	25.4 ± 0.3	148	26.0 ± 0.3	1	0°	15.3 ± 0.2
							90°	90.8 ± 4.4
PLA/ <i>v</i> CF10	55	118	28.0 ± 1.0	148	30.0 ± 0.5	2	0°	12.5 ± 1.5
							90°	84.6 ± 5.2

*Crystallization and melting enthalpy (ΔH_{cc} and ΔH_m) are normalized with the real polymer content in the composite material.

CLTE measurements are essential to assess the dimensional stability at different CFs content in 3D printed samples. In this context, CLTE value was calculated using samples produced with two filament deposition directions, namely, 0° and 90° with respect to the assessment direction. As shown in Table 4, neat PLA samples show an isotropic behaviour below the glass transition, as highlighted in the thermograms used for CLTE determination reported in Fig. 5a and b. The CLTE analysis in the two printing direction of all the composites materials (Fig. 5a and b and Table 4), instead, highlights that the CFs addition leads to a strong anisotropy in terms of thermal expansions, as already reported by Love et al [19]. While 90° composite 3D printed samples exhibit CLTE values not too distant from each other, with data slightly lower than neat PLA (in the range 84.5–97.5 10⁻⁶ 1/K) and almost unaffected by the CFs load, 0° specimens show a significant drop in the CLTE values. In particular, 5 wt% CFs content leads to a CLTE value drop by 65% with respect to neat PLA reference (Table 4), with almost no significant difference between washed *v*CFs and *r*CFs. Increasing the CFs load to 10 %wt, the thermal expansion of samples along the direction of filament deposition was reduced by over 85% when compared to the analogous neat PLA specimen. Such a behaviour can be ascribed to the presence of CFs, characterized by a slightly negative but practically invariant CLTE (−0.38 10⁻⁶ 1/K, from Toray T700 Technical Datasheet [45]), which hampers intermolecular mobility that cause the dilatation of the material leading to lower CLTE values [19].

Fig. 5



TMA thermograms of 3D printed samples in two directions: 0° (A) and 90° (B). The reported curves are relative to: (1) Neat PLA (—), (2) PLA/rCF5 (---), (3) PLA/vCF5 PLA (---), (4) PLA/rCF10 (---) and (5) PLA/vCF10 (---). Thermograms displayed in the figure are representative of each batch of specimens. (For interpretation of the references to colour in this figure legend, the reader is referred to the web version of this article.)

Storage modulus (E') and loss factor ($\tan\delta$) of 3D printed samples as a function of temperature were evaluated by DMA in tensile mode and results are displayed in Fig. 6. Specimens were 3D printed with a linear deposition pattern in the same direction of the applied forces during the analysis. The obtained results clearly highlight the significant stiffening effect due to CFs addition, which leads to a substantial increase of the storage modulus with CF content from about 2.3 GPa for neat PLA specimens up to 7.1 GPa for PLA/vCF10 (SI2-Table SII for the exact values). Beside the absolute E' value, other thermo-mechanical properties, as $T_{E'_{onset}}$ and $\tan\delta$ peak, show a slight increase when the CF loading is 10 wt%. In particular, the increase of $\tan\delta$ peak temperature as a function of CFs content is an evidence of the good interfacial adhesion between PLA and CFs, both *virgin* and *recycled*. It is worth to highlight the comparison between *r*CF and washed *v*CF reinforcement in both 5 and 10 wt% formulations. Indeed, the use of recycled CFs leads to a thermo-mechanical performance well comparable, or even slightly better than pristine fibers without any sizing on the surface, once again supporting the suitability of *r*CFs for 3D printing applications.


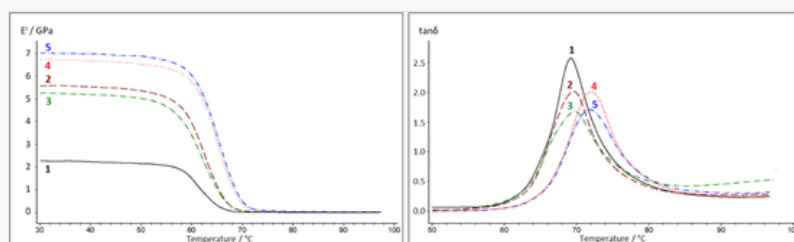
 Images are optimised for fast web viewing. Click on the image to view the original version.

Fig. 6



DMA thermograms of 3D printed samples: (A) Neat PLA (—), (B) PLA/rCF5 (---), (C) PLA/vCF5 PLA (---), (D) PLA/rCF10 (---) and (E) PLA/vCF10 (---). On the left the storage modulus (E' /MPa) vs temperature; on the right includes $\tan\delta$ vs temperature. Thermograms displayed in the figure are representative of each batch of specimens. (For interpretation of the references to colour in this figure legend, the reader is referred to the web version of this article.)

Finally, tensile tests of 3D printed dog-bone specimens were carried out according to ASTM D638 standard which involved a slow deformation rate (1 mm/min) for brittle materials, as CF reinforced plastics might end up being. Once again two directions of filament deposition, i.e. 0° and 90° with respect to the applied deformation, were evaluated.

Reference samples, consisting of neat PLA, show negligible effect of printing orientation on mechanical properties (Fig. 7a and b). According to the results summarized in Table 5, PLA samples 3D printed at 0° and 90° have similar Elastic Modulus and fracture behaviour showing a good isotropy and confirming the CTE results previously discussed. Such a behaviour suggests a suitable interbead adhesion for PLA since the layer-layer interface did not represent a weak point of the 3D printed samples, but it showed mechanical properties very close to samples produced aligning the filament in the direction of the applied load. CF-reinforced samples, instead, exhibit a strong anisotropy since 0° printed samples are more brittle, while 90° specimens show a more plastic behaviour, in particular *r*CF5. As seen by Bhandari et al. [21], 90° printed specimens (Table 5) show the weakening of interbead adhesion upon CFs addition. Indeed, 90° neat PLA specimens achieve $\sigma_b = 48$ MPa PLA/CFs composites just 30–40 MPa. Such an issue could be attributed to the fast cooling of CF-reinforced samples during printing process which hampers a proper welding of layers and, according to literature, to the enhanced melt viscosity of reinforced materials and the consequential slower interlayer diffusion bonding in composites [18,21]. Bringing the focus on intrinsic tensile properties of materials, i.e. 0° printed samples (Fig. 7a, c and e), the addition of CFs leads to the stiffening of samples, with elastic modulus going from 0.63 GPa for pure PLA up to 2.02 GPa for PLA/*r*CF10 (Table 5). The addition of 10 wt% recycled CFs to PLA leads, compared to neat PLA, to an increase of 50% in yield stress (σ_b), to a 220% increase in Young's modulus (E) and to a 60% decrease in strain at break (ϵ_b). These values fall in the average performance recorded for CF modified filaments [17,34]. Similarly to the work of Jiang et al. [17], these trends are explained by the high σ_b and E of the CF themselves and the anisotropic fiber-orientation along the 3D-printing direction, as already reported for the filaments (Fig. 2). Furthermore, the modulus and tensile strength measured for samples along their printing axis (0°) provides information about intrinsic material properties: in this case Table 5 reports a significant increase in both E and σ values when recycled fibers are used, with respect to washed virgin ones. It should be pointed out that the latter point occurs for *r*CFs with no additional surface treatment. Indeed, according to data summarized in Table 5, in both 5 and 10 wt% CFs formulations, recycled CFs had a higher efficiency in reinforcing PLA in terms of stiffness, and failure behaviour. Such a result could be explained by an enhanced interfacial adhesion between PLA matrix and the partially oxidized surface of recycled CFs that promotes an efficient load transfer [33,49].


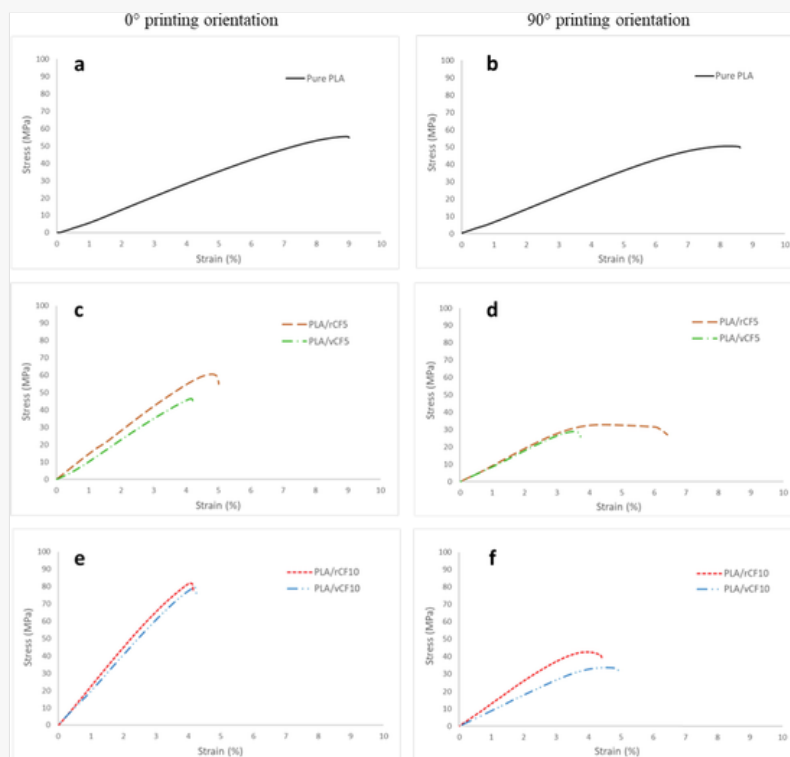
 Images are optimised for fast web viewing. Click on the image to view the original version.

Fig. 7



Tensile test of 3D printed dog-bone specimens with 2 printing orientation: 0° (first column: a, c and e) and 90° (second column: b, d and f). The reported curves are relative to: (a) and (b) neat PLA samples (—); (c) and (d) PLA/*r*CF5 (---) and PLA/*v*CF5 (---); (e) and (f) PLA/*r*CF10 (---) and PLA/*v*CF10 (---). Curves displayed in the figure are representative of each batch of specimens. (For interpretation of the references to colour in this figure legend, the reader is referred to the web version of this article.)

Table 5

The table layout displayed in this section is not how it will appear in the final version. The representation below is solely

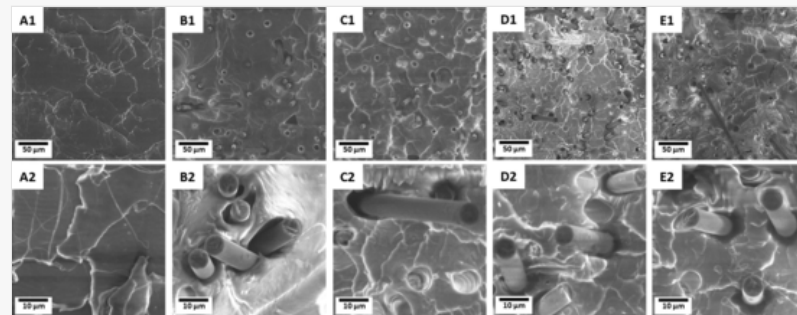
Tensile test results of 3D printed specimens.

Sample	Deposition angle	E (GPa)	σ_b (MPa)	ε_b (%)	σ_{yield} (MPa)
Neat PLA	0°	0.63 ± 0.07	54.5 ± 5.8	10.9 ± 0.4	
	90°	0.61 ± 0.05	48.0 ± 4.1	12.3 ± 1.6	
PLA/ <i>r</i> CF5	0°	1.56 ± 0.17	58.7 ± 2.0	5.0 ± 0.7	
	90°	0.96 ± 0.06	30.5 ± 0.9	6.1 ± 0.9	32.8 ± 1.7
PLA/ <i>v</i> CF5	0°	1.18 ± 0.09	46.5 ± 2.9	4.7 ± 0.3	
	90°	0.93 ± 0.03	26.8 ± 1.8	3.7 ± 0.2	
PLA/ <i>r</i> CF10	0°	2.02 ± 0.10	81.2 ± 0.6	4.4 ± 0.2	
	90°	1.03 ± 0.21	39.1 ± 3.2	4.5 ± 0.4	
PLA/ <i>v</i> CF10	0°	1.77 ± 0.16	77.8 ± 3.1	5.0 ± 0.5	
	90°	0.96 ± 0.17	30.7 ± 0.7	4.9 ± 0.1	

SEM micrographs (Fig. 8) of fracture surfaces of 0° 3D printed dog-bone specimen have been acquired in order to better evaluate the interfacial adhesion between fibers and matrix. At a first glance, PLA/CFs 3D printed specimens confirm the same fiber alignment as seen in the filament (Fig. 2) before printing, as all fibers are still oriented in the flow direction (Fig. 8). Moreover, the increment of CFs content, both recycled and virgin, from 5 wt% (Fig. 8A and B) to 10 wt% (Fig. 8C and D) leads to a densification of the fibers, still without causing agglomerates. Fibers are well dispersed and prevalently aligned. Pull out occurs, as highlighted by the empty cavities left by the fibers. The higher magnification of SEM micrographs of 5 and 10 %wt CF loaded samples also showed an empty cavity around many of the fibers emerging from the fractured surface, but the aspect of both *v*CFs and *r*CFs containing composites are practically identical. While analysing the 90° dogbone specimens' results (second column in Fig. 8) some interesting observations can be drawn: in the first instance I can be observed that in a situation where mostly interbead adhesion is affected by the applied stress direction, PLA/*r*CF composites show a better performance than the PLA/*v*CF counterparts. Another point to be raised is the observation that both 5 and 10% CF containing samples show a higher modulus and σ_b when the surface of the CF is slightly oxidized, so much that in the *r*CF5 a yield is observed in all the three different replicas, with evidence of plastic deformation instead of failure. The latter observation might suggest that the better adhesion in between PLA and the fibers upon oxidation can in turn drive a better adhesion in between adjacent beads, at least up to fibers concentration low enough so that the sample is not extremely stiffened. Such a better adhesion might then lead to further stiffening effects growing the CF content, as observed in the *r*CF10 when compared to *v*CF10.

i Images are optimised for fast web viewing. Click on the image to view the original version.

Fig. 8



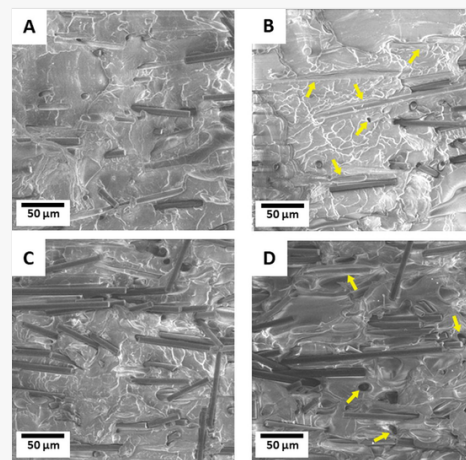
SEM micrographs of fracture surfaces of neat PLA (A), PLA/*r*CF5 (B), PLA/*v*CF5 (C), PLA/*r*CF10 (D) and PLA/*v*CF10 (E). The numbering of images indicates the used magnification: 1 for 1000× and 2 for 5000×.

The observation of fracture surfaces of the 90° dogbone specimens' (Fig. 9) once again display the high directionality conferred by the initial filament extrusion and further boosted by the printing process, as well as the efficient dispersion of CFs that is maintained even when the CF load is increased from 5 to 10 wt%. Moreover, the fact that upon fracture

in the *r*CF composites fibers are still highly embedded in the polymer while in *v*CF containing specimen fibers are more naked and significant sign of pull out appears support once again for the latter case a lower fiber to PLA adhesion, ascribable to the lack of an oxygen rich layer on the CF surface.

 Images are optimised for fast web viewing. Click on the image to view the original version.

Fig. 9



SEM micrographs of fracture surfaces of specimens printed at 90°. The reported micrographs are relative to: (A) PLA/rCF5; (B) PLA/vCF5; (C) PLA/rCF10; (D) PLA/vCF10. Yellow arrows are used to highlight pull out cavities in fracture surfaces. (For interpretation of the references to colour in this figure legend, the reader is referred to the web version of this article.)

All in all, the above discussed results all point at affirming the suitability of recycled CFs in additive manufacturing applications, with performances comparable, or even better, than those of the virgin ones. Indeed, when the fiber aspect ratio is not a crucial detrimental point, the quality of recycled CF has now achieved performances that make them a better alternative to the pristine fibers, in particular when economic aspects are also taken into account.

4 Conclusion

In conclusion, this work demonstrates the applicability of recycled carbon fibers in fusion-based additive manufacturing to produce CF reinforced PLA composite materials, in a frame of circular economy. The investigation of PLA composites with different CF contents revealed a good CF dispersion and a convenient printability of the formulations. The strong alignment of short CFs along the extrusion direction produces a flawless printing using a commercial 3D printer, but also leads to a strong anisotropy in mechanical properties of 3D printed composites. The evidence of the anisotropic reinforcement, for both recycled and virgin CF composites, is confirmed comparing tensile performances of dogbones printed with deposition angle of 0° and 90°. Indeed, the composite including 10 %wt *r*CF 3D printed at 0° with respect to the applied stress direction, shows about a doubling of both elastic modulus and maximal stress, compared to 90° orientation. The results are particularly intriguing considering the ease of fabrication of a recycled CF reinforced filament suitable for FDM application. Moreover, all reported results in this paper confirm the total comparability of *r*CFs with washed *v*CFs in terms of thermal and mechanical properties and, consequently, the suitability of *r*CFs in additive manufacturing application as an environmental and economically sustainable alternative to virgin CFs where the uneven and generally shortened dimension of the fibers might represent a benefit, without a significant apparent drawback.

CRedit authorship contribution statement

Niccolò Giani: Investigation, Writing – original draft. **Laura Mazzocchetti:** Conceptualization, Methodology, Writing – review & editing, Supervision. **Tiziana Benelli:** Conceptualization, Methodology, Writing – review & editing, Supervision. **Francesco Picchioni:** Supervision, Resources. **Loris Giorgini:** Resources, Funding acquisition, Supervision.

Declaration of Competing Interest


The authors declare that they have no known competing financial interests or personal relationships that could have appeared to influence the work reported in this paper.

Acknowledgements

Appendix A Supplementary material

Supplementary data to this article can be found online at <https://doi.org/10.1016/j.compositesa.2022.107002>.

References

 The corrections made in this section will be reviewed and approved by a journal production editor. The newly added/removed references and its citations will be reordered and rearranged by the production team.

- [1] IndustryARC, Composite Materials Market – Forecast (2021–2026), 2020.
- [2] Koumoulos E.P., Trompeta A.-F., Santos R.-M., Martins M., Santos C.M.D., Iglesias V., et al. Research and development in carbon fibers and advanced high-performance composites supply chain in Europe: a roadmap for challenges and the industrial uptake. *J Compos Sci* 2019;3(3):86. doi:10.3390/jcs3030086.
- [3] Sauer M. Composites Market Report 2019. Frankfurt AVK: Carbon Compos; 2019.
- [4] Bledzki A.K., Seidlitz H., Goracy K., Urbaniak M., Rösch J.J. Recycling of carbon fiber reinforced composite polymers—review—part 1: Volume of production, recycling technologies, legislative aspects. *Polymers (Basel)* 2021;13(2):1–13. doi:10.3390/polym13020300.
- [5] Sommer V., Walther G. Recycling and recovery infrastructures for glass and carbon fiber reinforced plastic waste from wind energy industry: a European case study. *Waste Manag* 2021;121:265–275. doi:10.1016/j.wasman.2020.12.021.
- [6] Song Y.S., Youn J.R., Gutowski T.G. Life cycle energy analysis of fiber-reinforced composites. *Compos Part A Appl Sci Manuf* 2009;40(8):1257–1265. doi:10.1016/j.compositesa.2009.05.020.
- [7] Holmes M. Recycled carbon fiber composites become a reality. *Reinf Plast* 2018;62(3):148–153. doi:10.1016/j.repl.2017.11.012.
- [8] Naqvi S.R., Prabhakara H.M., Bramer E.A., Dierkes W., Akkerman R., Brem G. A critical review on recycling of end-of-life carbon fibre/glass fibre reinforced composites waste using pyrolysis towards a circular economy. *Resour Conserv Recycl* 2018;136:118–129. doi:10.1016/j.resconrec.2018.04.013.
- [9] Giorgini L., Benelli T., Mazzocchetti L., Leonardi C., Zattini G., Minak G., et al. Recovery of carbon fibers from cured and uncured carbon fiber reinforced composites wastes and their use as feedstock for a new composite production. *Polym Compos* 2015;36(6):1084–1095. doi:10.1002/pc.23440.
- [10] Mazzocchetti L., Benelli T., Zattini G., Brancolini G., Giorgini L. Evaluation of carbon fibers structure and morphology after their recycling via pyro- gasification of CFRPs. *AIP Conf Proc* 2019;2196(December):1–5. doi:10.1063/1.5140309.
- [11] Mazzocchetti L., Benelli T., Angelo E.D., Leonardi C., Zattini G., Giorgini L. Validation of carbon fibers recycling by pyro-gasification: The influence of oxidation conditions to obtain clean fibers and promote fiber/matrix adhesion in epoxy composites. *Compos Part A Appl Sci Manuf* 2018;112:504–514. doi:10.1016/j.compositesa.2018.07.007.
- [12] Karuppanan Gopalraj S., Kärki T. A review on the recycling of waste carbon fibre/glass fibre-reinforced composites: fibre recovery, properties and life-cycle analysis. *SN Appl Sci* 2020;2(3):1–21. doi:10.1007/s42452-020-2195-4.
- [13] Pimenta S., Pinho S.T. Recycling carbon fibre reinforced polymers for structural applications: technology review and market outlook. *Waste Manag* 2011;31(2):378–392. doi:10.1016/j.wasman.2010.09.019.

- [14] Giorgini L., Benelli T., Brancolini G., Mazzocchi L. Recycling of carbon fiber reinforced composite waste to close their life cycle in a cradle-to-cradle approach. *Curr Opin Green Sustain Chem* 2020;26:100368. doi:10.1016/j.cogsc.2020.100368.
- [15] McConnell V.P. Launching the carbon fibre recycling industry. *Reinf Plast* 2010;54(2):33–37. doi:10.1016/S0034-3617(10)70063-1.
- [16] Duty C., Ajinjeru C., Kishore V., Compton B., Hmeidat N., Chen X., et al. What makes a material printable? A viscoelastic model for extrusion-based 3D printing of polymers. *J Manuf Process* 2018;35:526–537. doi:10.1016/j.jmapro.2018.08.008.
- [17] Jiang D., Smith D.E. Anisotropic mechanical properties of oriented carbon fiber filled polymer composites produced with fused filament fabrication. *Addit Manuf* 2017;18:84–94. doi:10.1016/j.addma.2017.08.006.
- [18] Zhang W., Cotton C., Sun J., Heider D., Gu B., Sun B., et al. Interfacial bonding strength of short carbon fiber/acrylonitrile-butadiene-styrene composites fabricated by fused deposition modeling. *Compos Part B Eng* 2018;137:51–59.
- [19] Love L.J., Kunc V., Rios O., Duty C.E., Elliott A.M., Post B.K., et al. The importance of carbon fiber to polymer additive manufacturing. *J Mater Res* 2014;29(17):1893–1898. doi:10.1557/jmr.2014.212.
- [20] Tekinalp H.L., Kunc V., Velez-Garcia G.M., Duty C.E., Love L.J., Naskar A.K., et al. Highly oriented carbon fiber-polymer composites via additive manufacturing. *Compos Sci Technol* 2014;105:144–150. doi:10.1016/j.compscitech.2014.10.009.
- [21] Bhandari S., Lopez-Anido R.A., Gardner D.J. Enhancing the interlayer tensile strength of 3D printed short carbon fiber reinforced PETG and PLA composites via annealing. *Addit Manuf* 2019;30:100922. doi:10.1016/j.addma.2019.100922.
- [22] Papon E.A., Haque A. Fracture toughness of additively manufactured carbon fiber reinforced composites. *Addit Manuf* 2019;26:41–52. doi:10.1016/j.addma.2018.12.010.
- [23] Seifans A.M., Ayyagari S., Al-Haik M. Elastic/viscoplastic characterization of additively manufactured composite based on continuous carbon fibers. *Aerosp Sci Technol* 2021;111:106562. doi:10.1016/j.ast.2021.106562.
- [24] Chen Y., Ye L. Topological design for 3D-printing of carbon fibre reinforced composite structural parts. *Compos Sci Technol* 2021;204:108644. doi:10.1016/j.compscitech.2020.108644.
- [25] Turner B.N., Strong R., Gold S.A. A review of melt extrusion additive manufacturing processes: I. Process design and modeling. *Rapid Prototyp J* 2014;20:192–204. doi:10.1108/RPJ-01-2013-0012.
- [26] Turner B.N., Strong R., Gold S.A. A review of melt extrusion additive manufacturing processes: II. Process design and modeling. *Rapid Prototyp J* 2015;21:250–261. doi:10.1108/RPJ-02-2013-0017.
- [27] Sangeetha V.H., Deka H., Varghese T.O., Nayak S.K. State of the Art and Future Prospectives of Poly(Lactic Acid) Based Blends and Composites. *Polym Compos* 2018;39(1):81–101. doi:10.1002/pc.23906.
- [28] Iwata T., Doi Y. Morphology and enzymatic degradation of poly(L-lactic acid) single crystals. *Macromolecules* 1998;31:2461–2467. doi:10.1021/ma980008h.
- [29] Tsuji H., Ikada Y. Blends of aliphatic polyesters. II. Hydrolysis of solution-cast blends from poly(L-lactide) and poly(ϵ -caprolactone) in phosphate-buffered solution. *J Appl Polym Sci* 1998;67:405–415. doi:10.1002/(SICI)1097-4628(19980118)67:3<405::AID-APP3>3.0.CO;2-Q.
- [30] Acik G. Preparation of antimicrobial and biodegradable hybrid soybean oil and poly (L-lactide) based polymer with quaternized ammonium salt. *Polym Degrad Stab* 2020;181:109317. doi:10.1016/j.polymdegradstab.2020.109317.

- [31] Karimi-Avargani M., Bazooyar F., Biria D., Zamani A., Skrifvars M. The special effect of the *Aspergillus flavus* and its enzymes on biological degradation of the intact polylactic acid (PLA) and PLA-Jute composite. *Polym Degrad Stab* 2020;179:109295. doi:10.1016/j.polymdegradstab.2020.109295.
- [32] van de Werken N., Tekinalp H., Khanbolouki P., Ozcan S., Williams A., Tehrani M. Additively manufactured carbon fiber-reinforced composites: state of the art and perspective. *Addit Manuf* 2020;31:100962. doi:10.1016/j.addma.2019.100962.
- [33] Brenken B., Barocio E., Favaloro A., Kunc V., Pipes R.B. Fused filament fabrication of fiber-reinforced polymers: a review. *Addit Manuf* 2018;21:1–16. doi:10.1016/j.addma.2018.01.002.
- [34] Ferreira R.T.L., Amatte I.C., Dutra T.A., Bürger D. Experimental characterization and micrography of 3D printed PLA and PLA reinforced with short carbon fibers. *Compos Part B Eng* 2017;124:88–100. doi:10.1016/j.compositesb.2017.05.013.
- [35] Zander N.E., Gillan M., Lambeth R.H. Recycled polyethylene terephthalate as a new FFF feedstock material. *Addit Manuf* 2018;21:174–182. doi:10.1016/j.addma.2018.03.007.
- [36] Zander N.E., Gillan M., Burckhard Z., Gardea F. Recycled polypropylene blends as novel 3D printing materials. *Addit Manuf* 2019;25:122–130. doi:10.1016/j.addma.2018.11.009.
- [37] Giani N., Ortolani J., Mazzocchetti L., Benelli T., Picchioni F., Giorgini L. Production of thermoplastic composite filaments for additive manufacturing using recycled Carbon Fibers. *Macromol Symp* 2021. in press.
- [38] Chen R., Misra M., Mohanty A.K. Injection-moulded biocomposites from polylactic acid (PLA) and recycled carbon fibre: Evaluation of mechanical and thermal properties. *J Thermoplast Compos Mater* 2014;27(9):1286–1300. doi:10.1177/0892705712471360.
- [39] Gańczyk-Specjalska K., Magnuszewska P. An analysis of the mechanical properties of HTPB-propellants using DMA. *High Energy Mater* 2020;12(2):81–91.
- [40] Blok L.G., Longana M.L., Yu H., Woods B.K.S. An investigation into 3D printing of fibre reinforced thermoplastic composites. *Addit Manuf* 2018;22:176–186. doi:10.1016/j.addma.2018.04.039.
- [41] Li N., Li Y., Liu S. Rapid prototyping of continuous carbon fiber reinforced polylactic acid composites by 3D printing. *J Mater Process Tech* 2016;238:218–225. doi:10.1016/j.jmatprotec.2016.07.025.
- [42] D’Urso L., Acocella M.R., Guerra G., Iozzino V., De Santis F., Pantani R. PLA melt stabilization by high-surface-area graphite and carbon black. *Polymers (Basel)* 2018;10(2):1–13. doi:10.3390/polym10020139.
- [43] Huxtable S.T., Cahill D.G., Shenogin S., Xue L., Ozisik R., Barone P., et al. Interfacial heat flow in carbon nanotube suspensions. *Nat Mater* 2003;2(11):731–734. doi:10.1038/nmat996.
- [44] Spoerk M., Savandaiah C., Arbeiter F., Traxler G., Cardon L., Holzer C., et al. Anisotropic properties of oriented short carbon fibre filled polypropylene parts fabricated by extrusion-based additive manufacturing. *Compos Part A Appl Sci Manuf* 2018;113:95–104.
- [45] Toray, T700S Technical Data Sheet, 2018.
- [46] Wang S., Chen Z.H., Ma W.J., Ma Q.S. Influence of heat treatment on physical-chemical properties of PAN-based carbon fiber. *Ceram Int* 2006;32(3):291–295. doi:10.1016/j.ceramint.2005.02.014.
- [47] Walker P.L., McKinstry H.A., Wright C.C. X-ray diffraction studies of a graphitized carbon – changes in interlayer spacing and binding energy with temperature. *Ind Eng Chem* 1953;45(8):1711–1715.
- [48]

Hong J.-H., Park D.-W., Shim S.-E. A review on thermal conductivity of polymer composites using carbon-based fillers: carbon nanotubes and carbon fibers. Carbon Lett 2010;11(4):347–356.

- [49] Kada D., Koubaa A., Tabak G., Migneault S., Garnier B., Boudenne A. Tensile properties, thermal conductivity, and thermal stability of short carbon fiber reinforced polypropylene composites. Polym Compos 2018;39(S2):E664–E670. doi:10.1002/pc.24093.

Highlights

- Recycled Carbon Fibers (*r*CF) can be easily dispersed in the thermoplastic matrix.
 - Composite filaments with *r*CF showed the same processability of *v*CF ones.
 - Recycling process of CFs did not affect mechanical properties of composites.
 - *r*CF can replace virgin CFs for eco-sustainable FDM applications.
-

Appendix A Supplementary material

The following are the Supplementary data to this article:



[Multimedia Component 1](#)

Supplementary Data 1

Queries and Answers

Q1

Query: Please review the **given names and surnames** to make sure that we have identified them correctly and that they are presented in the desired order. Carefully verify the spelling of all authors' names as well. If changes are needed, please provide the edits in the author section. /

Answer: Reviewed

Q2

Query: Your article is being processed as a regular item to be included in a regular issue. Please confirm if this is correct or if your article should be published in a special issue using the responses below. /

Answer: Yes

Q3

Query: Please check the **address for the corresponding author** that has been added here, and correct if necessary. /

Answer: Reviewed

Q4

Query: Correctly acknowledging the primary **funders and grant IDs** of your research is important to ensure compliance with funder policies. Please make sure that funders are mentioned accordingly. /

Answer: Reviewed

